ELSEVIER

Polymer 43 (2002) 2787–2794

polymer

www.elsevier.com/locate/polymer

Relaxation behaviour of thermoplastic polyurethanes with covalently attached nitroaniline dipoles

P. Frübing[a,*], H. Krüger[b,1], H. Goering[c], R. Gerhard-Multhaupt[a]

[a]*Department of Physics, University of Potsdam, Am Neuen Palais 10, D-14469 Potsdam, Germany*
[b]*Fraunhofer Institute for Reliability and Microintegration, Kantstrasse 55, D-14513 Teltow, Germany*
[c]*Federal Institute for Materials Research and Testing, Unter den Eichen 87, D-12205 Berlin, Germany*

Received 28 September 2001; accepted 14 January 2002

Abstract

Thermoplastic polyurethanes with covalently attached nitroaniline chromophores exhibit a strong high-temperature relaxation associated with a glass transition rather than the typical frequency-independent loss due to the aggregation of polymer chains via hydrogen bonds. This relaxation behaviour suggests the formation of an amorphous structure without separation into soft-segment and hard-segment phases. In such a structure, a field-induced orientation of molecular dipoles is stabilised by the high viscosity of the material below its glass transition. The dipole orientation yields a pyroelectric effect caused by dipole-density changes upon thermal expansion and contraction.

The changes in phase separation are investigated by varying the chain length of the soft-phase component and studying its influence on the calorimetric, dynamic-mechanical, and dielectrical properties. Good correlation was found between differential scanning calorimetry, dynamic-mechanical analysis and dielectric spectroscopy as well as measured and calculated pyroelectric coefficients. This leads to a uniform picture of the structural changes caused by the incorporation of nitroaniline chromophores into the polyurethane structure.

Keywords: Thermoplastic polyurethane; Nitroaniline chromophore; Dielectric relaxation

1. Introduction

Thermoplastic polyurethanes (TPUs) are microphase-separated systems composed of so-called hard- and soft-segment phases. The latter phase consists mainly of polyethers or polyesters and is less polar. It is usually mainly amorphous; crystallisation can, however, occur if soft segments of sufficient chain lengths are used. Furthermore, a glass transition is observed within its amorphous portion. A hard segment is composed of the diisocyanate component and the so-called chain extender, a low-molecular-weight diol. For particular chemical structures, the hard segments are able to aggregate, forming separate microdomains with a regular crystallite-like structure consisting of chain segments aligned in parallel. The domains are stabilised by hydrogen bonds between the NH group as donor and the carbonyl of another urethane group as acceptor. The hard phase is more polar because of the parallel alignment of the urethane dipoles [1].

Microphase separation is never complete because the soft and the hard segments are covalently linked. However, its degree can be adjusted over a wide range via the parameters of synthesis and film preparation as well as by using different hard-phase components or by varying the relative lengths of soft and hard segments. Microphase separation strongly influences the morphology as well as the mechanical, thermal and electrical properties. Considerable work has been done in this area. Recently, Georgoussis et al. [2] studied phase separation in TPUs with metal chelates incorporated in the PU chains. These systems are particularly interesting as potential ionic conductors. In addition, Georgoussis et al. [3] investigated molecular mobility and phase separation in TPUs with crown ethers as chain extenders. Their results suggest that the addition of crown ethers promotes microphase separation. Related studies with other chain extenders are reported by Savelyev et al. [4] and by Pissis et al. [5].

In recent years, polyurethanes were also suggested and studied as materials for piezo- and pyroelectrical applications. They are easier to process than the commonly used

* Corresponding author. Tel.: +49-331-977-1456; fax: +49-331-977-1577.
E-mail address: fruebing@rz.uni-potsdam.de (P. Frübing).
[1] Address: Fraunhofer Institute for Applied Polymer Research, Geiselbergstrasse 69, D-14476 Golm, Germany.

0032-3861/02/$ - see front matter
PII: S0032-3861(02)00075-7

polyvinylidene fluoride (PVDF). Zhang et al. [6] reported a very high electrostrictive coefficient, about two orders of magnitude higher than that of PVDF, in a commercial polyurethane elastomer. Pyroelectricity was found in aliphatic [7] as well as in aromatic [8] polyurethanes. It is assumed that a field-induced orientation of urethane dipoles can be stabilised or even a spontaneous polarisation be generated in these materials through the formation of hydrogen bonds between segments of different chains, as it was found in odd-numbered polyamides [9].

Here, TPUs were synthesised with the chain extender partly substituted by a strong molecular dipole in order to increase the electric polarisation of the hard phase. The length of the soft segments has been varied. Differential scanning calorimetry (DSC), dynamic-mechanical analysis (DMA), dielectric spectroscopy as well as pyroelectrical measurements were employed to study the influence of the resulting structural variations on molecular mobility, phase separation, thermal stability and electrical polarisation.

2. Sample preparation and experimental procedures

The chemical structures of the polyurethane components are shown in Fig. 1. Polyoxytetramethylene (polytetrahydrofurane (PTHF)) forms the soft segment. The hard segment is composed of 4,4′-methylene bis(phenylisocyanate) (MDI) and of the chain extender butane-1,4-diol (BD 1.4), which is partly substituted by the OH-bifunctional nitroaniline derivative bis-(2-hydroxyethyl)amino-4-nitrobenzene (BHEANB). Together with the amino group as electron donor and the nitro group as acceptor, the benzene ring with its delocalised π-electron system forms a strong dipole (A–π–D dipole) with a dipole moment of 8.5 ± 0.4 D calculated by means of molecular modelling with the AM1 module of the Spartan program package. The BHEANB was synthesised from 4-fluoro-nitrobenzene and diethanolamine in water. The reaction mixture was refluxed for 8 h. The resulting yellow crystals were purified by repeated recrystallisation from ethanol. The purity was checked with chromatography. The substance was identified with ^{1}H and ^{13}C NMR and by means of FTIR spectroscopy.

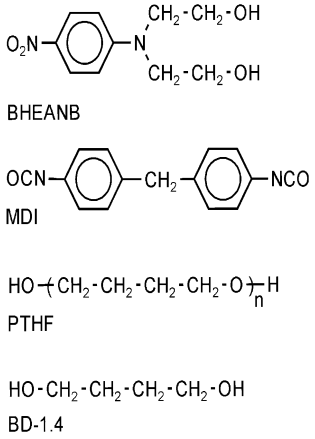

Fig. 1. Chemical components of the thermoplastic polyurethanes with molecular dipoles. $n = 15$, 30 and 45 for PTHF 1000, PTHF 2000 and PTHF 3000, respectively.

All components were carefully dried. MDI was freshly distilled in vacuum before polyurethane synthesis. The polyurethanes were obtained in a one-shot process in dimethylformamide (DMF) solution by stirring for 3 h at 70 °C under nitrogen. Free-standing, yellow-coloured, transparent films with thickness ranging from 20 to 110 μm were prepared from the solution by coating with a doctor blade onto glass substrates. The films were annealed for at least 1 h at 130 °C in order to evaporate the solvent, then taken off the glass substrates by means of immersion in de-ionised water, and finally dried in vacuum at 50 °C. The films are thermally stable up to 250 °C as determined with thermogravimetry.

Films based on PTHFs with molecular masses of either 1000 g/mol (PTHF 1000) or 2000 g/mol (PTHF 2000) or 3000 g/mol (PTHF 3000) and reference films without nitroaniline dipoles were prepared. The molar composition of the dipole-containing films is 1 mol PTHF, 17.34 mol MDI, 8 mol BD1.4, and 8 mol BHEANB; that of the dipole-free films is 1 mol PTHF, 6.12 mol MDI, and 5 mol BD1.4. The resulting concentrations N_{HS} of hard segments (HS) and N_D of BHEANB dipoles are listed in Table 1.

The DSC investigations were carried out in a Mettler-Toledo DSC 821e over a temperature range from −30 to 250 °C with heating and cooling rates of 20 K/min. All DSC measurements were repeated, only the second runs are presented.

DMA measurements were performed with a Rheovibron DDV-II-B, Toyo Baldwin, in tensile mode on film strips of $40 \times 5 \times 0.2$ mm^3 at a frequency of 3.5 Hz and a heating rate of 2.0 K/min. All DMA measurements were taken on as-prepared samples without any special pretreatment.

For electrical measurements, aluminium electrodes (thickness 50 nm, electrode area $A = 1.00$ cm^2) were vacuum evaporated onto both sides of the films. The dielectric spectra were recorded in a temperature range from −150 to +170 °C and a frequency range from 20 Hz to 1 MHz with an HP 4284A precision impedance meter. As with DMA, only as-prepared samples were used. The

Table 1
Relative concentrations of hard-segment phase N_{HS} and BHEANB dipoles N_D in the films used for the present investigation

Soft segment	Dipole-free; N_{HS} (wt%)	Dipole-containing	
		N_{HS} (wt%)	N_D (wt%)
PTHF 1000	65.2	86.7	22.8
PTHF 2000	46.8	75.3	19.8
PTHF 3000	38.8	68.7	18.1

samples were cooled or heated in a nitrogen-gas stream by use of a Novocontrol cryosystem QUATRO. The data were acquired as a function of frequency under nearly isothermal conditions ($\Delta T_{max} = 0.25$ K) and through a series of ascending temperatures (5 K steps).

Pyroelectric coefficients were determined from quasi-static pyroelectric measurements [10]. To this end, the films were poled in a dc field E_p at a constant elevated temperature T_p for a time t_p and subsequently cooled to room temperature under field. Then the electrodes were shorted through a Keithley 617 electrometer, and finally the sample was exposed to a slow sinusoidal temperature oscillation. The poling as well as the current measurement was performed in dry nitrogen. A purpose-build sample holder with low heat capacity was used together with the Novocontrol cryosystem QUATRO. The experimental pyroelectric coefficient p_{exp} — defined as the temperature derivative $p_{exp} = (1/A)(dQ/dT)$ of the charge density Q/A induced on the electrodes — can be calculated from the total current through the film as

$$p_{exp} = \frac{J_0 \sin \theta}{\omega T_0}. \quad (1)$$

Here, ω and T_0 are the angular frequency and the amplitude of the sinusoidal temperature oscillation, respectively; J_0 is the amplitude of the current density, and θ is the phase shift between the oscillations of the total current and the temperature. The pyroelectric current is phase shifted by $\theta = \pi/2$ with respect to the temperature, whereas non-pyroelectric currents due to relaxation and conduction are always in phase with the temperature. Thus, the true pyroelectric current can be well identified with this method.

DSC, DMA and dielectric spectroscopy are sensitive to thermodynamic phase transitions such as melting and crystallisation or the glass transition of the amorphous phase. Shape, intensity and location of the signals that are connected with these processes depend on the method and on the experimental conditions, in particular the heating rate and the frequency. Here, only qualitative comparisons are made, quantitative comparisons would require a systematic variation of these parameters.

3. Results and discussion

3.1. Differential scanning calorimetry

DSC thermograms of films based on PTHF 1000, PTHF 2000 and PTHF 3000 without and with BHEANB dipoles are presented in Figs. 2 and 3, respectively. A step of the heat flow at about 15 °C which is visible in all cooling curves does not represent a polymer property. It is generated by the equipment which does not allow for controlled cooling below room temperature.

The peaks that are visible in the thermogram of the PTHF 3000-based dipole-free material are attributed to melting and crystallisation of hard segments (melting at 180–220 °C) as well as within the soft phase (melting at about +20 °C). Obviously, the melting of hard segments is not a uniform process, which indicates a molecular-mass distribution within the hard phase. Furthermore, the chains of PTHF 3000 are sufficiently long so that partial crystallisation is possible also in the soft phase. At shorter chain lengths (PTHF 2000 and PTHF 1000-based films), this process is suppressed: only a very small endothermal peak is visible in the thermogram of the PTHF 2000-based film.

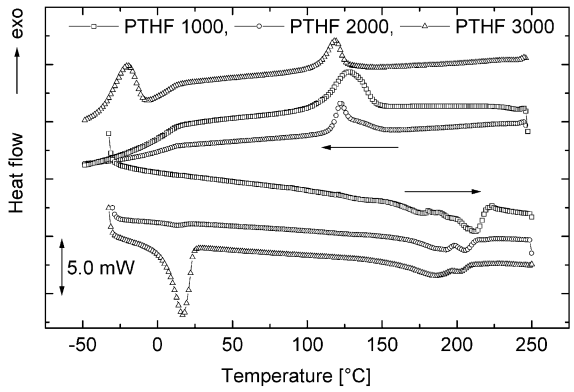

Fig. 2. DSC thermogram of dipole-free films with different PTHF components as indicated.

The dipole-containing films (Fig. 3) show quite different behaviour. Melting of the PTHF crystallites is detected only on the PTHF 3000-based film around 20 °C, but no melting of hard-segment aggregates is found. Obviously, the incorporation of BHEANB dipoles sterically hinders the aggregation of hard segments and produces an almost completely amorphous material. Glass transitions can be observed at 96.8 °C on the PTHF 1000-based film and at 108.7 °C on the PTHF 2000-based film.

3.2. Dynamic-mechanical analysis

Young's modulus as well as the mechanical loss factor tan δ of films based on PTHF 1000, PTHF 2000 and PTHF 3000 without and with molecular dipoles are presented in

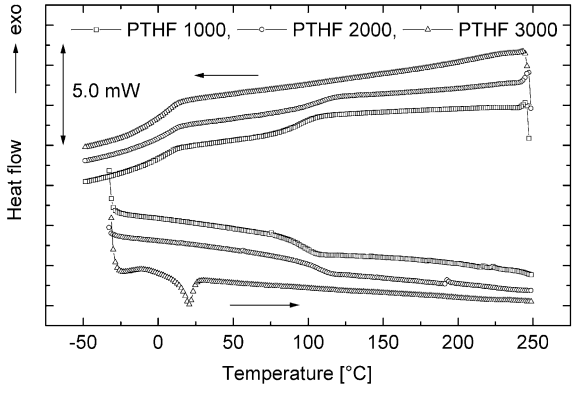

Fig. 3. DSC thermogram of dipole-containing films with different PTHF components as indicated.

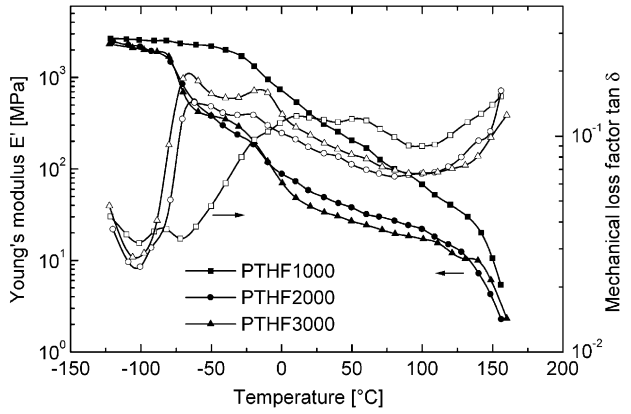

Fig. 4. Temperature dependence of Young's modulus (solid symbols) and of the mechanical loss factor (open symbols) at $f = 3.5$ Hz for dipole-free TPUs with different PTHF components as indicated.

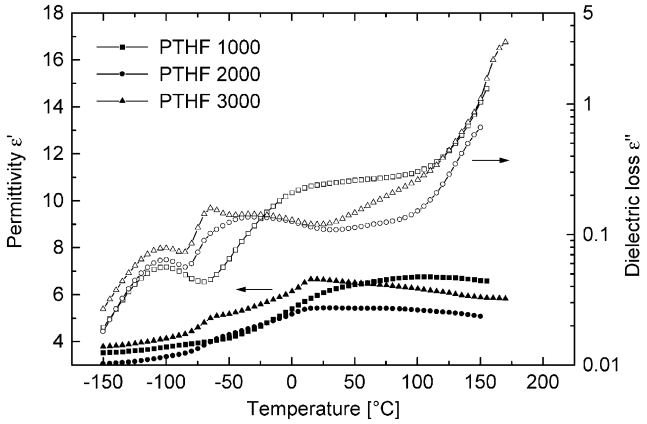

Fig. 6. Temperature dependence of the permittivity (solid symbols) and of the dielectric loss (open symbols) at $f = 2.0$ kHz for dipole-free TPUs with different PTHF components as indicated.

Figs. 4 and 5, respectively. The modulus of the dipole-free PTHF 3000-based TPU clearly shows three steps accompanied by the corresponding maxima of the loss factor. The first step at about −75 °C is attributed to the glass transition within the soft phase. The second step at about −20 °C stems from melting of crystallites formed by the PTHF. The third step at about 150 °C is attributed to melting of well-ordered hard-segment domains. In the dipole-free PTHF 2000-based film, the glass transition within the soft phase becomes broader and the crystallisation process within the soft phase is less pronounced. The dipole-free PTHF 1000-based film shows only a faster decay of the modulus above −50 °C, but no glass transition and no melting of crystallites within the soft phase can be recognised. Obviously, the PTHF chains are so short and the hard-segment content is so high in this case (cf. Table 1) that these processes are suppressed.

The dipole-containing PTHF 3000-based TPU (Fig. 5) also shows the glass transition of the soft-segment phase (modulus step at about −70 °C) and the melting of PTHF crystallites (modulus step at about −10 °C). In contrast, these processes are not found on the PTHF 2000- and PTHF 1000-based dipole-containing films. Their moduli remain nearly constant up to a pronounced relaxation with loss peaks at 104 and 91 °C, respectively. Obviously, this relaxation corresponds to the glass transition found in DSC. Furthermore, particularly the PTHF 3000-based film does not show a drop of the modulus above 150 °C, i.e. no melting of any hard-segment domains. The plateau modulus above the glass transition is caused by stable entanglements. These features indicate a mixed phase structure similar to a block copolymer without phase separation.

3.3. Dielectric spectroscopy

The permittivity ϵ' as well as the dielectric loss ϵ'' of dipole-free and of dipole-containing films are shown in Figs. 6 and 7, respectively. On the dipole-free films, the development of phase separation is clearly visible. The permittivity of the PTHF 3000-based dipole-free film

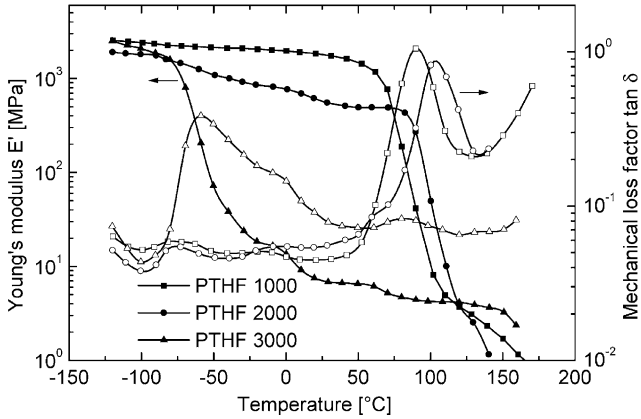

Fig. 5. Temperature dependence of Young's modulus (solid symbols) and of the mechanical loss factor (open symbols) at $f = 3.5$ Hz for dipole-containing TPUs with different PTHF components as indicated.

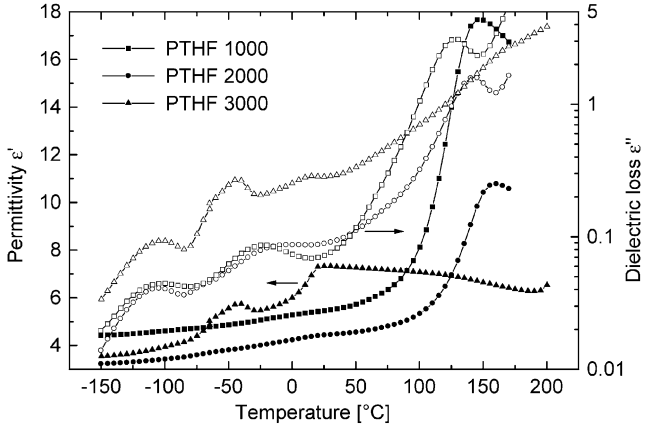

Fig. 7. Temperature dependence of the permittivity (solid symbols) and of the dielectric loss (open symbols) at $f = 2.0$ kHz for dipole-containing TPUs with different PTHF components as indicated.

shows two steps around −65 and 20 °C which indicate the glass transition within the soft phase and the melting of crystallites formed in the soft phase, respectively. According to the Kramers–Kronig relations, the steps in ϵ' are accompanied by maxima of ϵ''. An additional loss maximum occurs at about −100 °C. Similar, but not so well pronounced steps of ϵ' in the spectrum of the PTHF 2000-based dipole-free film indicate that the glass transition within the soft phase and the melting of soft-phase crystallites still occur, whereas the PTHF 1000-based TPU exhibits only gradual increases of ϵ' and ϵ'' in this temperature range, which indicates that these processes are suppressed, as already found with DMA.

The PTHF 3000-based dipole-containing film shows a similar behaviour as its dipole-free reference film. As also seen with DMA, the glass transition within the soft phase is even more pronounced. Furthermore, the melting of PTHF crystallites is clearly detected. It is shifted to higher temperatures compared to DMA because DMA was carried out at a much lower frequency than dielectric spectroscopy. Therefore, in DMA all relaxation processes appear at significantly lower temperatures, and the temperature shifts depend on the particular temperature dependence of the relaxation time.

The dielectric spectra of the PTHF 2000- and PTHF 1000-based dipole-containing films look quite different. First, ϵ' and ϵ'' are significantly lower at temperatures where the glass transition within the soft phase and the melting of soft-phase crystallites of the PTHF 3000-based films occur. In the PTHF 2000-based film, only a weak PTHF-crystallisation process is detected as a flat step of ϵ' at about 20 °C. Second, a strong relaxation is present with loss maxima at 143 and 130 °C and corresponding steps in ϵ' of about 5 and 12, respectively. Obviously, this relaxation corresponds to the earlier-described mechanical loss-factor maximum found with DMA at 104 and 91 °C as well as to the glass transition recorded with DSC at 109 and 97 °C, respectively.

For a more detailed analysis of the new high-temperature relaxation process, the permittivity is fitted with a Havriliak–Negami (HN) function:

$$\epsilon(\omega) = \frac{\Delta\epsilon}{[1 + (i\omega\tau)^{\alpha}]^{\beta}} + \epsilon_{\infty}, \tag{2}$$

with $\omega = 2\pi f$, $\Delta\epsilon$ the relaxation strength, τ the relaxation time, α and β the shape parameters describing the width and the asymmetry of the loss maximum, respectively, and ϵ_{∞} the unrelaxed permittivity. The result is presented in Fig. 8. It was obtained after subtracting a conductivity term of the form $\epsilon'' = [\sigma_0/(\epsilon_0\omega)]^n$, were σ_0 and n are fit parameters and ϵ_0 is the permittivity of free space. The relaxation parameters obtained from the HN fits are given in Figs. 9 and 10. The following features of this relaxation are visible:

1. The relaxation strength is relatively high (above 10).

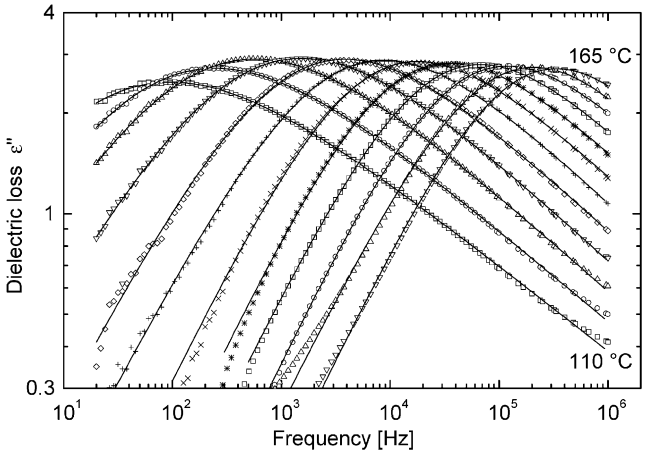

Fig. 8. Isothermal plots of the high-temperature loss maximum of the dipole-containing PTHF 1000-based TPU at temperatures from 110 to 165 °C in steps of 5 K (symbols) together with Havriliak–Negami fits (solid lines).

2. The loss maximum is asymmetric, and it narrows with increasing temperature.
3. The relaxation time obeys the Vogel–Fulcher–Tammann–Hesse (VFTH) law:

$$\tau = \tau_0 \exp\frac{T_a}{T - T_V}, \tag{3}$$

where τ_0 is a reciprocal frequency factor, T_a the activation temperature and T_V the Vogel temperature.

These features are typical for a segmental relaxation associated with the glass transition in amorphous polymers. The dynamic glass-transition temperature is defined as the temperature where the relaxation time is 100 s [11]. The extrapolation of the straight line in Fig. 10 to $\tau = 100$ s gives $T_g = 79.4$ °C. Even though this value is lower than expected from the DSC measurements, it can be concluded that the high-temperature relaxation is related to the onset of

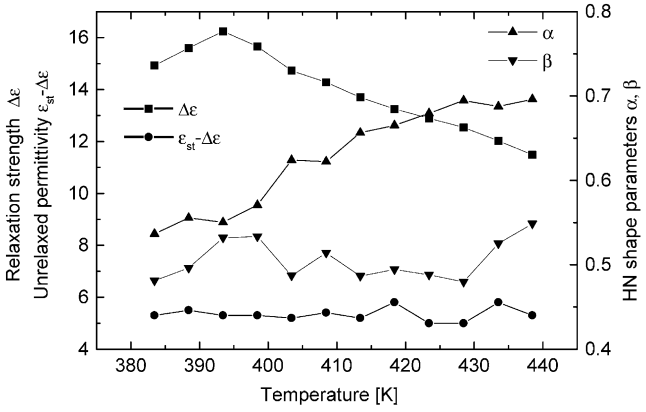

Fig. 9. Temperature dependence of the parameters $\Delta\epsilon$, ϵ_{∞}, α and β of the Havriliak–Negami fits shown in Fig. 8 (dipole-containing PTHF 1000-based TPU). The lines are only given in order to guide the eyes.

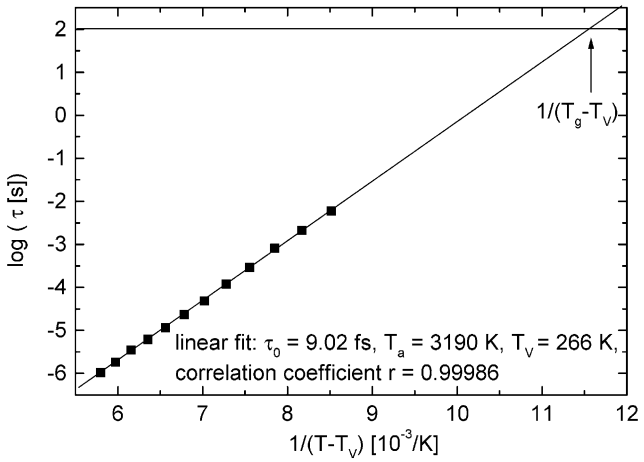

Fig. 10. Vogel–Fulcher–Tammann–Hesse plot of the parameter τ of the Havriliak–Negami fits shown in Fig. 8 (dipole-containing PTHF 1000-based TPU).

co-operative segmental motions of polyurethane chains with incorporated BHEANB dipoles in an amorphous environment.

The low-temperature relaxation (loss maximum at about −100 °C) has not been investigated in detail. It was found on all films regardless of whether they contained BHEANB dipoles or not. Because of its temperature range, it can be identified as the γ relaxation associated with motions of $(CH_2)_n$ sequences [12].

3.4. Pyroelectrical measurements

The dielectric-spectroscopy results suggest that the dipole-containing PTHF 2000- and PTHF 1000-based films may be dipole electrets after poling above the glass-transition temperature and subsequent cooling down. In particular, they should be pyroelectric due to BHEANB dipole-density changes upon thermal expansion and contraction [13].

A typical pyroelectric measurement on a PTHF 1000-based dipole-containing film is presented in Fig. 11. The

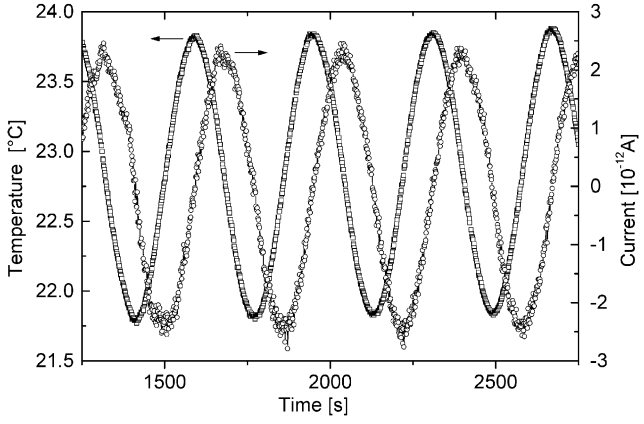

Fig. 11. Sinusoidal temperature oscillation and pyroelectrical current of a PTHF 1000-based dipole-containing film. For further explanations see text.

film was poled at $E_p = 30$ MV/m and $T_p = 100$ °C for $t_p = 30$ min. The measurement was carried with $\omega = 0.0175\ s^{-1}$ and $T_0 = 1.0$ K at a mean temperature of 25 °C. The current is almost exclusively pyroelectric (phase shift $\theta \approx \pi/2$). With Eq. (1), a pyroelectric coefficient of $p_{exp} = 1.3\ \mu C/(m^2 K)$ is determined.

The pyroelectric coefficient of a dipole electret can also be calculated theoretically with an equation for the total polarisation P that was first derived by Mopsik and Broadhurst [14] on the basis of the Onsager cavity model:

$$P = \frac{\epsilon_\infty + 2}{3} N_D \mu \langle \cos \Theta \rangle, \tag{4}$$

where N_D is the dipole concentration, μ the permanent dipole moment, and $\langle \cos \Theta \rangle$ is the average tilt of the dipole moments. The pyroelectric coefficient is defined as $p = dP/dT = d(Q/A)/dT$. Since the change in electrode area is difficult to determine, we use the experimental pyroelectric coefficient $p_{exp} = (1/A)(dQ/dT)$. Evaporated electrodes of a free-standing film deform with the film upon heating and cooling. Thus, differentiating and neglecting the term with $d\langle \cos \Theta \rangle/dT$, one obtains:

$$p_{exp} = \frac{\epsilon_\infty + 2}{3} \alpha P, \tag{5}$$

where $\alpha = (1/L)dL/dT$ is the coefficient of linear thermal expansion and L is the film thickness. The polarisation is calculated from the dielectric strength $\Delta\epsilon$ and the poling field as follows:

$$P = \epsilon_0\, \Delta\epsilon E_p. \tag{6}$$

The linear thermal-expansion coefficient can be determined from the slope of the displacement versus temperature below the glass-transition temperature in DMA: a value of $\alpha = 2.5 \times 10^{-4}\ K^{-1}$ is found. The other quantities follow from dielectric spectroscopy. With $\Delta\epsilon = 11.6$ (100 °C), $\epsilon_\infty = 5.4$ and $E_p = 30$ MV/m, a polarisation of $P = 3.1\ mC/m^2$ and a pyroelectric coefficient of $p_{exp} = 1.9\ \mu C/(m^2\ K)$ are calculated. With the improved relation

$$p_{exp} = \left(\frac{\epsilon_\infty + 2}{3} - \frac{2}{5} \right) \alpha P, \tag{7}$$

suggested by Winkelhahn et al. [15] who took the affine motion of the dipoles with the deforming matrix upon compression or expansion into consideration, $p_{exp} = 1.6\ \mu C/(m^2\ K)$ is calculated which is even closer to the directly measured value. Thus, it is concluded that the pyroelectric effect is mainly caused by BHEANB dipole-density changes upon thermal expansion and contraction. Unfortunately, higher poling fields were not possible because of electrical breakdown. The relatively low electrical breakdown strength is probably related to a high ionic conductivity at elevated temperatures [8].

After Eq. (4), the maximum possible dipolar polarisation

(saturation polarisation) is given by

$$P_{sat} = \frac{\epsilon_\infty + 2}{3} N_D \mu, \quad (8)$$

which means perfect dipolar orientation, the film being one macro-domain. The dipole concentration can be calculated from the molecular masses of the TPU components, the molar composition (see above) and the sample density (1020 kg/m^3). With $N_D = 6.08 \times 10^{26}$ m^{-3} (for PTHF 1000-based material) and $\mu = 2.84 \times 10^{-29}$ C m (8.5 D), we find $P_{sat} = 43$ mC/m^2 and $p_{exp} = 26.3$ μC/(m^2 K). Thus, only 7% of the polarisation theoretically possible at saturation are achieved before electrical breakdown. Finally, the temporal stability of the pyroelectric coefficient was checked. An exponential decay with a half-life of 2.9 days was found.

On the PTHF 2000-based films, a pyroelectric coefficient of $p_{exp} = 1.4$ μC/(m^2 K) was detected for $T_p = 110$ °C and otherwise identical poling conditions. Here, the polarisation is significantly lower (cf. Fig. 7: $\Delta\epsilon \approx 6$), but the dipole mobility and thus the change in polarisation upon thermal expansion should be higher. As expected, no pyroelectric activity was found on the PTHF 3000-based film at room temperature (poling at 190 °C, 10 MV/m, 30 min) because there is no relaxation which can be frozen in. This supports the results of the other experiments presented above. Furthermore, it indicates that the urethane dipoles do not contribute significantly to the observed polarisation and pyroelectricity, even though their individual dipole moments are 2.0 D (dipole moment of the isolated urethane group calculated by means of the AM1 module of the Spartan program package) and their concentration is about four times higher than that of BHEANB. Probably, the urethane dipoles cannot rotate freely because they are parts of the polyurethane chain and also because they are linked to each other via hydrogen bonds.

4. Summary and conclusions

DSC, DMA, dielectric spectroscopy and quasistatic pyroelectrical measurements have been employed for the investigation of phase separation and dipole orientation in films of TPUs with covalently attached nitroaniline dipoles. The molecular weight of the PTHF which forms the soft phase has been varied. The four methods give a clear and uniform picture of the processes going on at the molecular level.

A formation of hard-segment domains takes place in all dipole-free films. In addition, the PTHF 3000-based film shows melting and crystallisation as well as a glass transition within the soft phase. The other dipole-free films have obviously so short PTHF chains and so high hard-segment content, that these processes are partly (PTHF 2000-based films) or entirely (PTHF 1000-based films) suppressed.

In all the dipole-containing films, the hard segments do not aggregate. These films show a mixed phase structure similar to a block copolymer rather than the typical phase separation of TPUs. Furthermore, a high-temperature glass transition was found in the PTHF 2000 and PTHF 1000-based films. It is associated with a pronounced segmental relaxation, its strength is mainly determined by the dipole moment and the concentration of the BHEANB dipoles. This relaxation can be used to render the film pyroelectric at room temperature by electrical poling. The magnitude of the pyroelectric effect is of the same order as in other amorphous dipole electrets. It can be calculated by use of data obtained from DMA and dielectric spectroscopy. However, poling is not very efficient. Probably, the size of the BHEANB dipoles is too large and/or they cannot be sufficiently stabilised by freezing only. In addition, the electrical breakdown strength of the films is not sufficient for more efficient poling.

Higher and application-relevant pyroelectric coefficients can only be expected for phase-separated structures with a non-vanishing net dipole moment of the hard-segment domains. A variation of the chemical structure is only one way to achieve this. Equally important are physical methods of generating ordered supramolecular structures like annealing and stretching which were very successfully applied to render polymers like PVDF and odd-numbered polyamides ferroelectric.

Acknowledgements

The authors are indebted to Prof. Dr Siegfried Bauer (University of Linz) for stimulating discussions, to Katarina Padaszus for carrying out the TPU synthesis and the DSC measurements, and to Reinhard Hentschke (MPI for Polymer Research, Mainz) for calculating the dipole moment of the BHEANB. Financial support from the Stiftung Industrieforschung (Project U43/97) is gratefully acknowledged.

References

[1] Goering H, Krüger H, Bauer M. Multimodal polymer networks: design and characterisation of nanoheterogeneous PU elastomers. Macromol Mater Engng 2000;278:23–35.

[2] Georgoussis G, Kanapitsas A, Pissis P, Savelyev YV, Veselov VY, Privalko EG. Structure–property relationships in segmented polyurethanes with metal chelates in the main chain. Eur Polym J 2000;36:1113–26.

[3] Georgoussis G, Kyritsis A, Pissis P, Savelyev YV, Arhranovich ER, Privalko EG, Privalko VP. Dielectric studies of molecular mobility and microphase separation in segmented polyurethanes. Eur Polym J 1999;35:2007–17.

[4] Savelyev YV, Arhranovich ER, Grekov AP, Privalko EG, Korskanov VV, Shtompel VI, Privalko VP, Pissis P, Kanapitsas A. Influence of chain extenders and chain end groups on properties of segmented polyurethanes. I. Phase morphology. Polymer 1998;39:3425–9.

[5] Pissis P, Kanapitsas A, Savelyev YV, Arhranovich ER, Privalko EG, Privalko VP. Influence of chain extenders and chain end groups on properties of segmented polyurethanes. II. Dielectric study. Polymer 1998;39:3431–5.

[6] Zhang QM, Su J, Kim CH, Ting R, Capps R. An experimental investigation of electromechanical responses in a polyurethane elastomer. J Appl Phys 1997;81:2770–6.
[7] Tasaka S, Shouku T, Asami K, Inagaki N. Ferroelectric behavior in aliphatic polyurethanes. J Appl Phys 1994;33:1376–9.
[8] Jayasuriya AC, Tasaka S, Inagaki N. Pyroelectric properties of linear aromatic polyurethanes. IEEE Trans Diel Electr Insul 1996;3:765–9.
[9] Esayan S, Scheinbeim JI, Newman BA. Pyroelectricity in Nylon 7 and Nylon 11 ferroelectric polymers. Appl Phys Lett 1995;67:623–5.
[10] Garn LE, Sharp EJ. Use of low-frequency sinusoidal temperature waves to separate pyroelectric currents from nonpyroelectric currents. J Appl Phys 1982;53:8974–80.
[11] Donth E. Relaxation and thermodynamics in polymers. Berlin: Akademie-Verlag, 1992. p. 141 and 181.
[12] McCrum NG, Read BE, Williams G. Anelastic and dielectric effects in polymeric solids. London: Wiley, 1967. p. 499.
[13] Bauer S, Lang SB. Pyroelectric polymer electrets. In: Gerhard-Multhaupt R, editor. Electrets, 3rd ed., vol. 2, 1999. p. 129–92 (chapter 12).
[14] Mopsik FI, Broadhurst MG. Molecular dipole electrets. J Appl Phys 1975;46:4204–8.
[15] Winkelhahn H-J, Winter HH, Neher D. Piezoelectricity and electrostriction of dye-doped polymer electrets. Appl Phys Lett 1994;64:1347–9.